*Article*

# Carbon-Dioxide-Assisted Gasification of Sunflower Husk: An Impact of Iron, Nickel, or Cobalt Addition

Artem A. Medvedev [1,2,*], Daria A. Beldova [1,2], Leonid M. Kustov [1,2], Mikhail Yu. Mashkin [1,2], Svetlana B. Polikarpova [3], Valentina Z. Dobrokhotova [3], Elena V. Murashova [1], Marina A. Tedeeva [1,2], Pavel V. Sokolovskiy [1,2] and Alexander L. Kustov [1,2]

[1] N. D. Zelinsky Institute of Organic Chemistry RAS, 119991 Moscow, Russia; dashabelk@yandex.ru (D.A.B.); lmkustov@mail.ru (L.M.K.); mikhail.y.mashkin@gmail.com (M.Y.M.); murashovaev@rambler.ru (E.V.M.); maritedeeva@mail.ru (M.A.T.); levap90@list.ru (P.V.S.); kyst@list.ru (A.L.K.)

[2] Chemistry Department, Moscow State University, 119992 Moscow, Russia

[3] N. V. Sklifosovskiy Institute of Clinical Medicine, I.M. Sechenov First Moscow State Medical University, 119991 Moscow, Russia; polikarpova_s_b@staff.sechenov.ru (S.B.P.); dobrokhotova_v_z@staff.sechenov.ru (V.Z.D.)

* Correspondence: artom.medvedev@yandex.ru

**Abstract:** While the attempts to find new energy sources have intensified, the interest in the use of biomass as a carbon-rich raw material still is increasing. In this work, we studied iron-, cobalt-, and nickel-based materials in the process of $CO_2$-assisted gasification of sunflower husk. The materials with and without metal additives were examined by XRD, SEM, EDX, and TEM techniques and were tested in their gasification under the action of $CO_2$. It was found that the Co-based material demonstrates the best activity among the studied ones (the $CO_2$ conversion was up to 83%). The possible reason for such superiority may be related to the capability of Ni compounds to the formation of the metallic nickel phase and insufficient activity of iron species.

**Keywords:** $CO_2$ utilization; carbon monoxide; biomass gasification; sunflower husk; heterogeneous catalysis; transition metal catalysis

## 1. Introduction

Search for new energy sources is a problem of high importance because of the predicted fossil fuels resources depletion [1]. That is why an intensive search for the alternatives should be conducted. A possible way is to use materials of bio-origin, which can partially substitute fossils. Another problem is a high level of $CO_2$ emissions affecting ecological environment, and one of the ways to recycle it is to use it as a gasifying agent. Gasification using $CO_2$ leads to a higher yield of carbon monoxide and hydrogen compared to traditional methods using water vapor [2–5]. Carbon dioxide is widely used in the chemical industry. $CO_2$ can be used as a raw material for the production of various chemical compounds, for example, urea. Dehydrogenation of propane using carbon dioxide is a progressive process that can be an effective way to produce propene. $CO_2$ is also used for the synthesis of methanol, which is a source of clean fuel and chemical raw materials.

A possible way to solve these problems ($CO_2$ and residues of biomass utilization) is the use of biomass wastes in a production of valuable compounds: they are rich in carbon and hydrogen. Additionally, the problem of $CO_2$ utilization can be partially resolved if $CO_2$ is used as a gasification agent. The necessity of research in the field of the effective and ecologically friendly catalysts investigation to produce valuable compounds like artificial fuels or at least CO stimulates scientists efforts [6].

Plethora of studies on the gasification of biomass residues and other substances like tar and char concern different aspects of the problem. The complex nature and diverse composition of any biomass makes its investigation and utilization very complex and

intricate. But the most used way instead is burning it to produce heat (and $CO_2$), so an effective catalytic system should be found for an alternative way of utilization. Biomass ashes nevertheless can also be applied as catalytic compounds [7].

A simplified scheme of the processes taking place during gasification can be described in the following Equation: $C_{(s)} + CO_{2(g)} = 2\,CO_{(g)}$. Additionally, the formation of methane was observed in a series of works; the possible source of hydrogen for its formation is hydrogen from organic biomass, containing quite large amounts of hydrogen along with oxygen and carbon.

Main efforts in development of catalytic processes of this type of the carbon wastes utilization are focused on the application of alkali metals [8–12], alkali-earth metals [13–15], transition metals [16–21], and even noble metal catalysis [22,23]. Different materials are used as carriers for carbon waste utilization, like clays [24–26], MgO [27], and so on, but the major efforts are devoted to the systems with metals directly deposited on the gasified (or pyrolyzed) material, including sunflower wastes [28–30].

Sunflower husk is a large-scale waste that is mostly produced by the vegetable oil industry [31]; its uses as a fossil and cellulosic materials lead to its investigation from the point of view of pelletizing for energy uses [32]. Here, we intended to study the other side of the problem—the use by transformation into gasses. There are examples of gasification of biomass to hydrogen-rich products using potassium carbonate [33], resulting in the high yields of the desired product. The immanent inorganic compounds affect the catalytic behavior [34], and it is also a point of the investigation here.

This work is aimed at the preparation and investigation of the catalytic systems based on sunflower husk to reveal the dependence of the metals of the iron triad nature and their amounts in the catalytic $CO_2$-assisted gasification.

## 2. Materials and Methods

### 2.1. Matrials

The following reagents were used in this work: $Fe(NO_3)_3 \cdot 9\,H_2O$ (99%), $Co(NO_3)_2 \cdot 6\,H_2O$ (99%), $Ni(NO_3)_2 \cdot 6\,H_2O$ (98%) from Acros Organics, sunflower husk, and bidistilled water. All the reagents were used as purchased without further purification. $CO_2$ used in the gasification process was of the grade 99.99%, produced by Hermes-Gas.

The element CHNS composition of sunflower husk was determined, and the results are presented in Table 1. It can be clearly seen that about 50 wt. % of the starting material consists of carbon.

**Table 1.** CHNS element composition of the starting sunflower husk.

| Element | C | H | N | S |
|---|---|---|---|---|
| Content, wt. % | $47.60 \pm 0.08$ | $6.05 \pm 0.12$ | $0.63 \pm 0.06$ | <0.1 |

### 2.2. Methods of Characterization

The catalysts were characterized by a series of physico-chemical methods both fresh and after pre-heating at 600 °C. A main reason of using pre-heating in $CO_2$, not inert gas, was to ex situ investigate the transformations the catalysts undergo during the reaction and, thus, estimate the effects not only of high temperature but also of a reaction mixture. A desired reaction of carbon substrate gasification occurs almost solely at the temperatures above 600 °C, so this temperature was chosen as a reference for the state of the pre-heated catalyst.

The samples were examined with scanning electron microscopy (SEM) on a LEO SUPRA 50 VP microscope (Carl Zeiss, Jena, Germany) with an Inca Energy 500 energy-dispersive detector under low vacuum in a nitrogen atmosphere. EDX data were collected using an energy-dispersive spectrometer INCA Energy (Oxford Instruments, X-Max-80, Abingdon, UK). For the study, a small amount of the sample (less than 1 mg) was applied to conductive tape on polished aluminum substrates and placed in the microscope chamber.

The chamber was evacuated to a residual pressure of $10^{-6}$ mmHg. The samples were then exposed to an electron beam, the energy of the primary electrons was 3–10 keV, and the current varied between 2 and 40 pA. The focal length of the electron beam varied between 5 and 15 mm. To evaluate the distribution of elements, the samples were mapped.

TEM-SAED studies were conducted using transmission electron microscope JEM 2100 (JEOL, Tokyo, Japan), and the accelerating voltage was 200 kV. The sample was preliminarily dispersed in isopropyl alcohol, then treated with ultrasound for 10 min. After obtaining a homogeneous suspension, the solution was dropped onto a copper grid with a carbon amorphous coating. After drying, the grid was loaded into the chamber of the transmission electron microscope. EDX and SAED data were collected using the energy-dispersive spectrometer from INCA Energy (Oxford Instruments, X-Max-80, Abingdon, UK).

Powder X-ray diffraction patterns were collected with a STOE STADI P transmission diffractometer (Chicago, IL, USA) using Cu K$\alpha_1$ radiation monochromatized with a curved germanium (111) monochromator. The samples were examined in the region of 2 q 10–80°, with a step of 0.01° and a 10 s counting time per point. Before the examination, the samples were heated at 600 °C for one hour in a flow of $CO_2$ of 30 mL per minute.

Elemental analysis CHNS was accomplished by dry combustion in a CHNSO-analyzer Leco TruSpec Micro (LECO, St. Joseph, MI, USA). The principle of the device operation is combustion of samples in oxygen of 99.999% purity at the temperature of 1075 °C. Detection: carbon—by $CO_2$ (IR cell), hydrogen—by $H_2O$ (IR cell), nitrogen—by $N_2$ (thermal conductivity detector), sulfur—by $SO_2$ (IR cell). Sample weights of $2.0 \pm 0.2$ mg were weighed on a BM 20 G analytical balance (AND, Tokyo, Japan) and then placed in $4 \times 3.2$ mm silver capsules and sealed. For each of the samples, this procedure was repeated three times (3 parallel experiments). Then, capsules with samples were placed in the autosampler of the instrument for measurements.

### 2.3. The Catalytic Characterization

The evaluation of the activities of the resulting materials in a gasification process was performed using a quartz flow-type reactor with the internal diameter of 8 mm under a $CO_2$ pressure of 1 atm; the temperature ramp was 10 °C per minute, the temperature range was 100–850 °C, and the total flow rate of $CO_2$ was 30 mL per minute. In the case of the experiments aimed at the estimation of the material balance, a larger amount of the material was used, 6 g. The $CO_2$ flow was also set at the value of 100 mL per minute. A Bronkhorst EL-FLOW SELECT F-111B gas flow controller was used to control the gas flow rate. The material loading was 1 g, and the particle size was 0.25–0.5 mm. The reaction gas products were analyzed using a Chromatek Crystal 5000 gas chromatograph with thermal conductivity detectors, M ss316 3 m $\times$ 2 mm columns, Hayesep Q 80/100 mesh, and CaA molecular sieves.

The conversion ($X$) of carbon dioxide during the tests was calculated by the following formula (Equation (1)):

$$X_{CO_2} = \frac{F_{CO_2}^{in} - F_{CO_2}^{out}}{F_{CO_2}^{in}}, \tag{1}$$

where $F$ indicates flows in and out of the reactor, $X$ is for $CO_2$ conversion value.

### 2.4. Preparation of the Catalytic Materials

The starting material was grinded using a coffee grinder to obtain the particles of the size of 0.25–0.5 cm. All the samples were prepared as follows: The nitrate of Fe, Co, or Ni was completely dissolved in the appropriate amount of water to make the overall volume of the solution equal to wet capacity of the material. The amount of sunflower husk (5 g) was impregnated with the appropriate salt solution amount to obtain the desired metal content (1, 3 or 5 wt. %) varying the concentration of the solution and conserving its volume used. The samples were dried at 50 °C overnight in an oven. So, the series of

samples was prepared and further designated as *nM*/SFH, where *n* was 1, 3, or 5 wt. % of metal loading, and *M* was Fe, Co, or Ni.

## 3. Results

### *3.1. Electron Microscopy*

Scanning electron microscopy photos clearly show the structure of the biomass (Figure 1): The channels can be seen resulting from the natural capillaries occurring in plants. The porous walls also can be noticed: such pores can enhance the surface area of the material and thus provide a higher dispersion of the active phase over the surface of the catalytic material at the beginning of the gasification process.
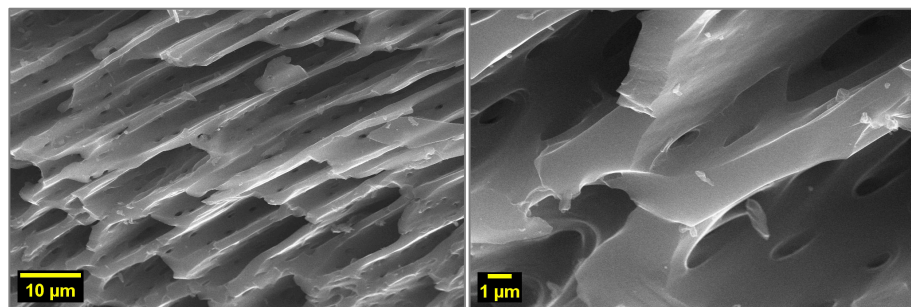


**Figure 1.** SEM images of sunflower husk heated at 600 °C in a $CO_2$ flow.

The compositions of the samples before and after the catalytic tests are given in Table 2. It can be seen that the composition of all the samples are quite close in the contents of the main elements. The slight drop in the added metal content can be tentatively explained as a result of the possible migration of their species into the depth of the grains, which is why they cannot be seen on the surface. Figure 2 also does not show any clear difference in morphology, it indicates the presence of a certain stability during the gasification process.

**Table 2.** Elemental composition of the samples before and after catalytic tests defined by EDX.

| Sample | Element Content, wt. % | | | | | | | | | | |
|---|---|---|---|---|---|---|---|---|---|---|---|
| | C | O | Mg | Si | P | S | K | Ca | Fe | Co | Ni |
| 5 Fe/SFH | 59.5 | 14.2 | 0.4 | — | 0.06 | 0.3 | 2.9 | 1.1 | 21.7 | — | — |
| 5 Fe/SFH spent | 56.9 | 15.5 | 0.5 | — | 0.04 | 0.3 | 2.4 | 1.3 | 23.2 | — | — |
| 5 Co/SFH | 47.2 | 13.7 | 1.3 | — | — | 0.4 | 3.8 | 2.0 | — | 31.6 | — |
| 5 Co/SFH spent | 66.0 | 9.4 | 0.3 | — | 0.12 | 0.3 | 1.7 | 0.9 | — | 21.3 | — |
| 5 Ni/SFH | 41.9 | 10.2 | 0.8 | — | — | 0.3 | 4.2 | 1.5 | 1.0 | — | 40.2 |
| 5 Ni/SFH spent | 35.4 | 11.9 | 0.5 | 0.2 | — | 2.1 | 7.0 | 1.0 | — | — | 42.0 |
| SFH | 54.5 | 43.2 | 0.4 | 0.1 | — | 0.1 | 0.4 | 1.6 | — | — | — |
| SFH spent | 59.6 | 33.9 | 2.1 | 0.2 | 0.1 | 0.8 | 2.3 | 1.2 | — | — | — |

Further investigation of sunflower husk was performed by using transmission electron microscopy (Figures 3 and 4). Despite the absence of any addition of the active metals to the material, the energy dispersion spectra indicate the presence of such elements in the sample as Mg, Si, K, Ca. All these elements occur naturally in the plants, and their presence makes us anticipate any intrinsic catalytic activity for such materials. Both pre-heated and spent materials demonstrate the presence of the particles of the elements with larger masses than the matrix (dark areas in microphotos), and they grow significantly during the catalytic tests.

The TEM images of the 'fresh' metal-loaded sunflower husk are shown in Figure 5. All the samples demonstrate the presence of the metallic (or metal oxide) particles in their photos. We can see both relatively small particles of about 10 nm and large ones of more than 200 nm. As can be seen, the particles of metals in the sample containing cobalt are larger in size than in other fresh samples.
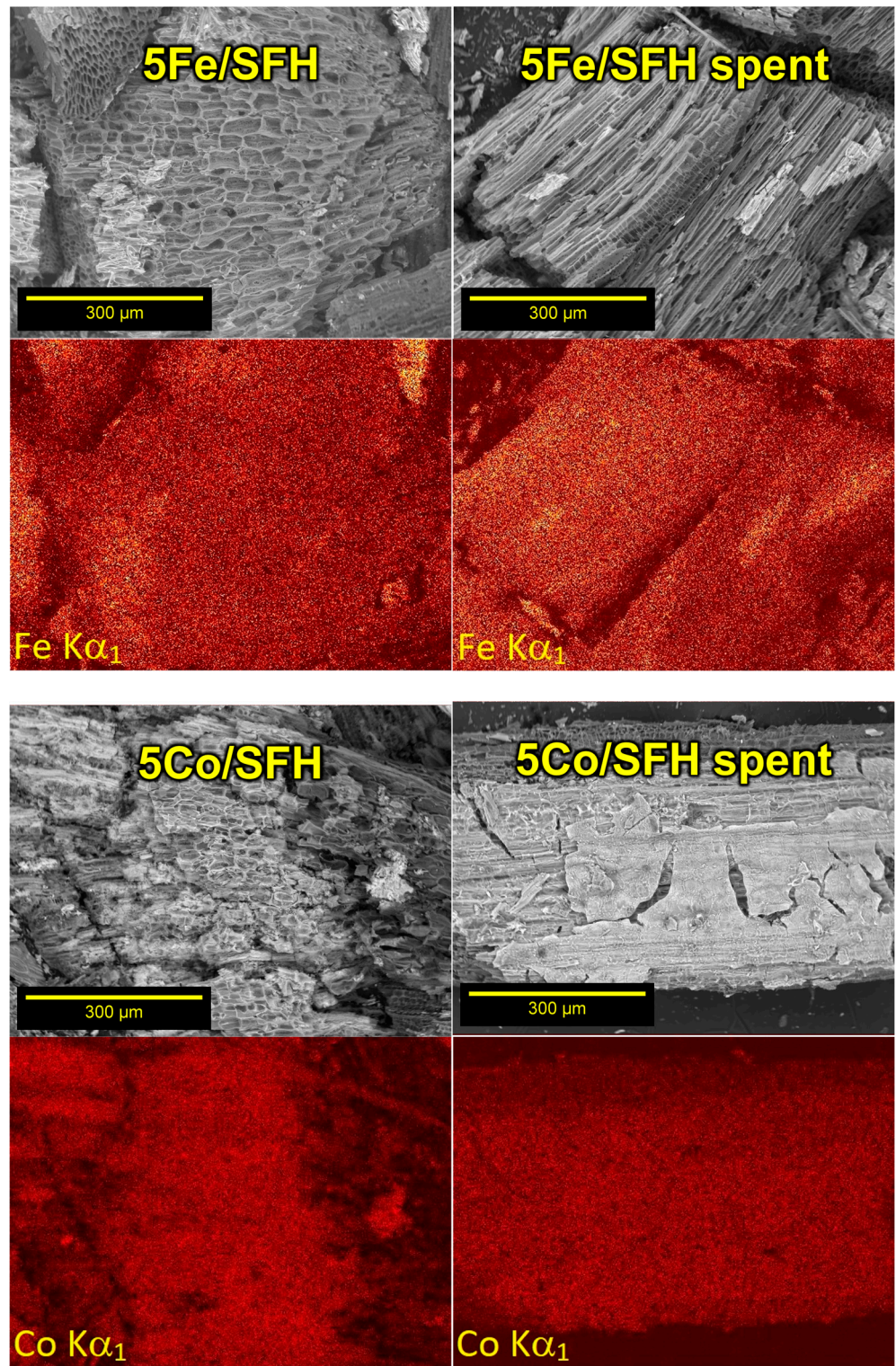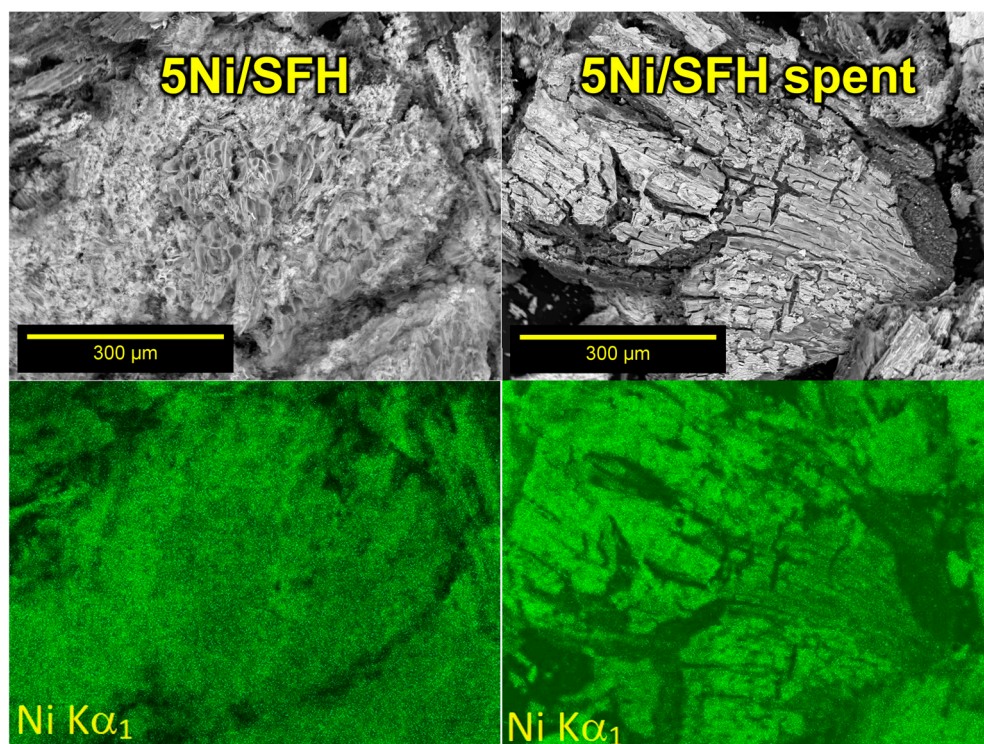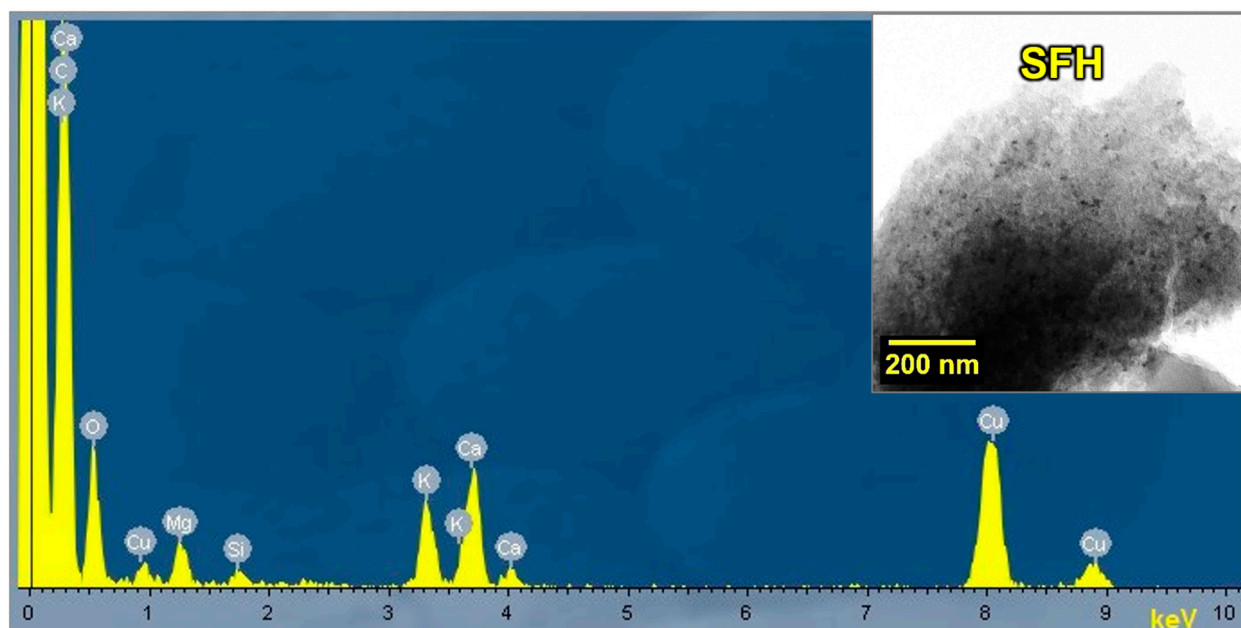
**Figure 2.** *Cont.*

**Figure 2.** SEM images and element maps (Fe, Co, or Ni) for the samples before and after catalytic tests.



**Figure 3.** TEM image of the fresh pre-heated sunflower husk (the insertion) and energy-dispersion spectrum (the main picture).

Figure 6 shows the samples after the catalytic experiments in $CO_2$-assisted gasification. The particles of metals grew up in their overall size, so it can be seen clearly for the nickel-containing sample. It is interesting to note that we can discover layer structures in Ni-based particles: the gray core is coated with dark metal-rich layer further coated with a lighter layer and so on. It can be described as a wood-like structure of the layers. The Co-containing sample still shows mostly the small particles. It can be suggested that such particles are also present in the other samples, but still there is a possibility that it is the specificity of the nature of metals. The iron-containing sample demonstrates the

particle size distribution in between. During the catalytic reaction, the distribution was slightly shifted, and the distribution became more uniform and symmetrical. It can be caused by the formation of more or less thermodynamically stable particle shapes and sizes, like Ostwald ripening. The decrease in particle size occurs due to the implementation of the carbide mechanism of the process under consideration [35]. Within the framework of this mechanism, carbon particles are coated along the perimeter with transition metal compounds, forming core–shell particles (such particles are clearly distinguishable in Ni-containing samples). During the process, carbon atoms from the carbon particles diffuse through the active phase of the material in the form of carbide and interacts with $CO_2$ on the carbide surface. During the described mechanism, carbon from the carbon-containing particles gradually burns out and increases the number of small particles.
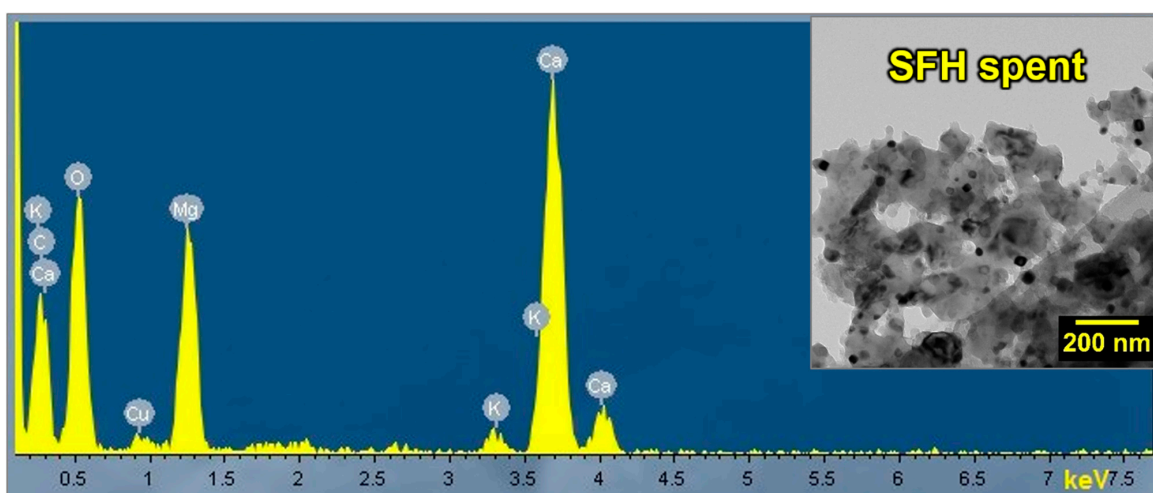


**Figure 4.** TEM image of the spent sunflower husk (the insertion) and energy-dispersion spectrum (the main picture).
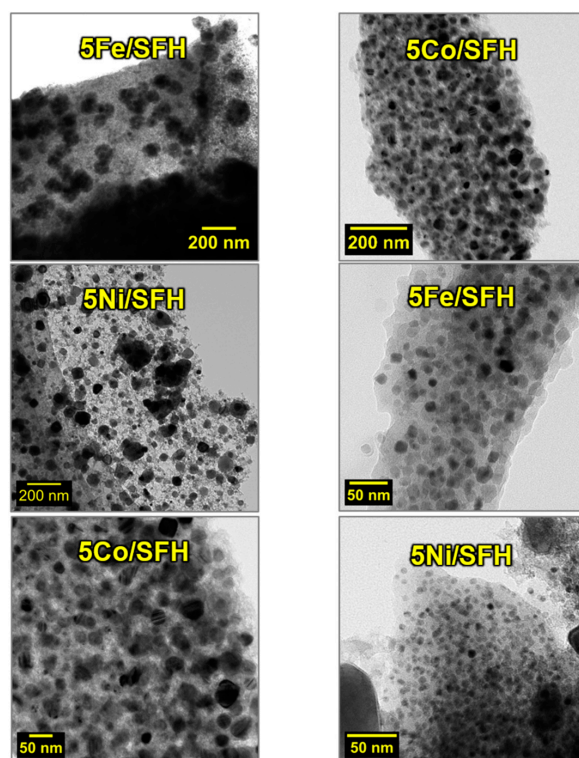


**Figure 5.** TEM images of the fresh catalytic materials heated at 600 °C for 1 h in a $CO_2$ stream.
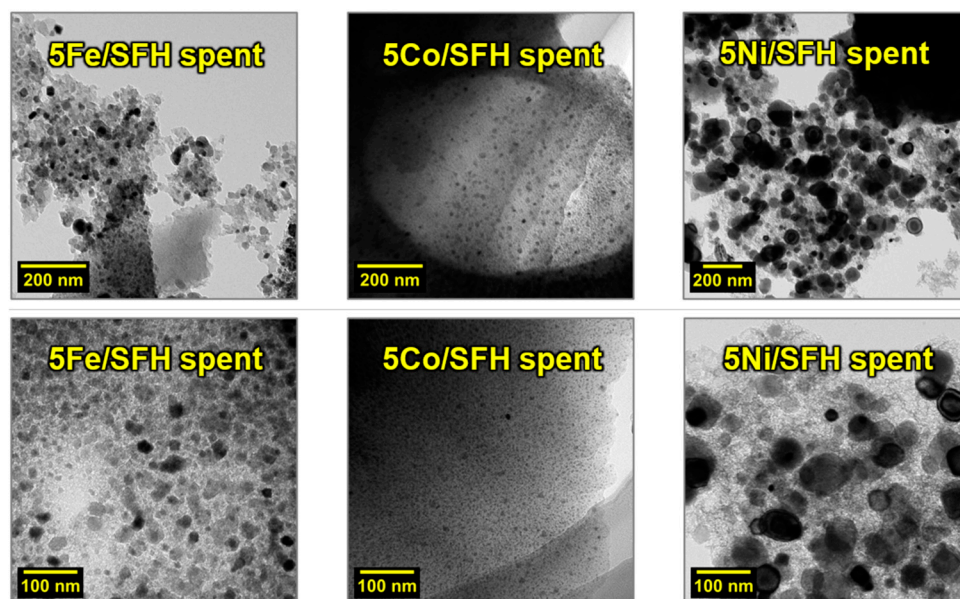
**Figure 6.** TEM images of the spent catalytic materials in $CO_2$-assisted gasification of sunflower husk.

The distributions of the metal-containing particles by size are presented in Figure 7. In the case of the iron-loaded sample, after the catalytic tests, the distribution of iron-containing particles becomes monomodal and narrower (10–50 nm), being compared with the distribution before the catalytic gasification of SFH, which showed the bimodal distribution in the range of 3–70 nm. It can be said that a more uniform distribution of the particles in size took place. The Co-loaded sample showed a dramatic decrease in the particle size; the initial wide distribution in the range of 1–120 nm was transformed into a monomodal distribution in the range of 1–20 nm. It may indicate a dramatic redistribution of Co species in the sample during the catalytic process. The Ni-loaded sample showed only slight changes after the catalytic test, and almost the same width of the distribution shifted to the larger sizes region for about 40 nm.
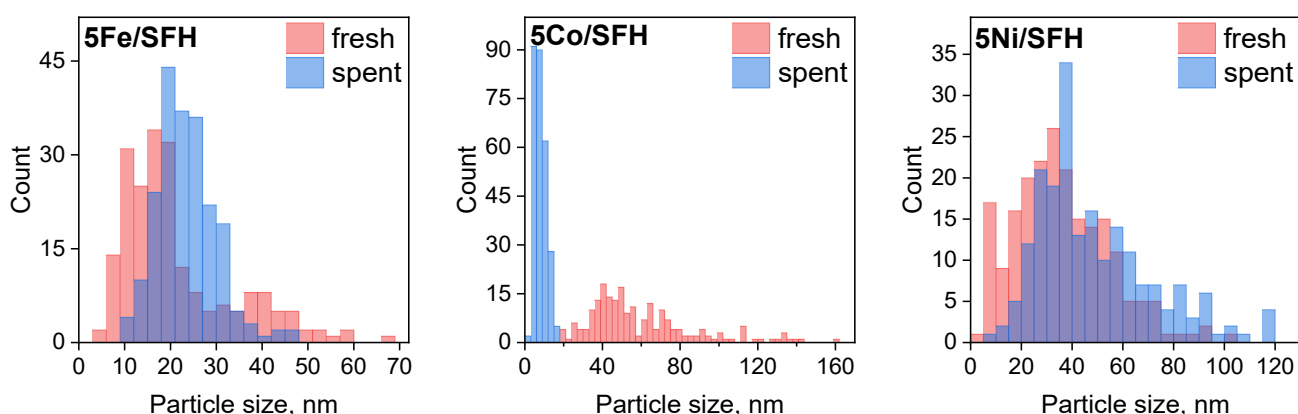


**Figure 7.** Metal-containing particle distributions by size for the materials impregnated with 5 wt. % Fe, Co, or Ni, before and after the catalytic tests.

### 3.2. Diffraction Patterns

The XRD pattern of the sample of pure sunflower husk after heating in a $CO_2$ flow at 600 °C (Figure 8) shows the only phase of $SiO_2$ cristobalite according to the ICDD card number [46–1242]. After the catalytic test in $CO_2$-assisted gasification, the intensity of the peak at ~34.7° slightly increased. The possible reason of that is the higher temperatures during gasification than the temperature of pre-heating (850 °C vs. 600 °C). The corresponding sizes of crystallites grow from 44 nm to 52 nm according to the Sherrer equation.
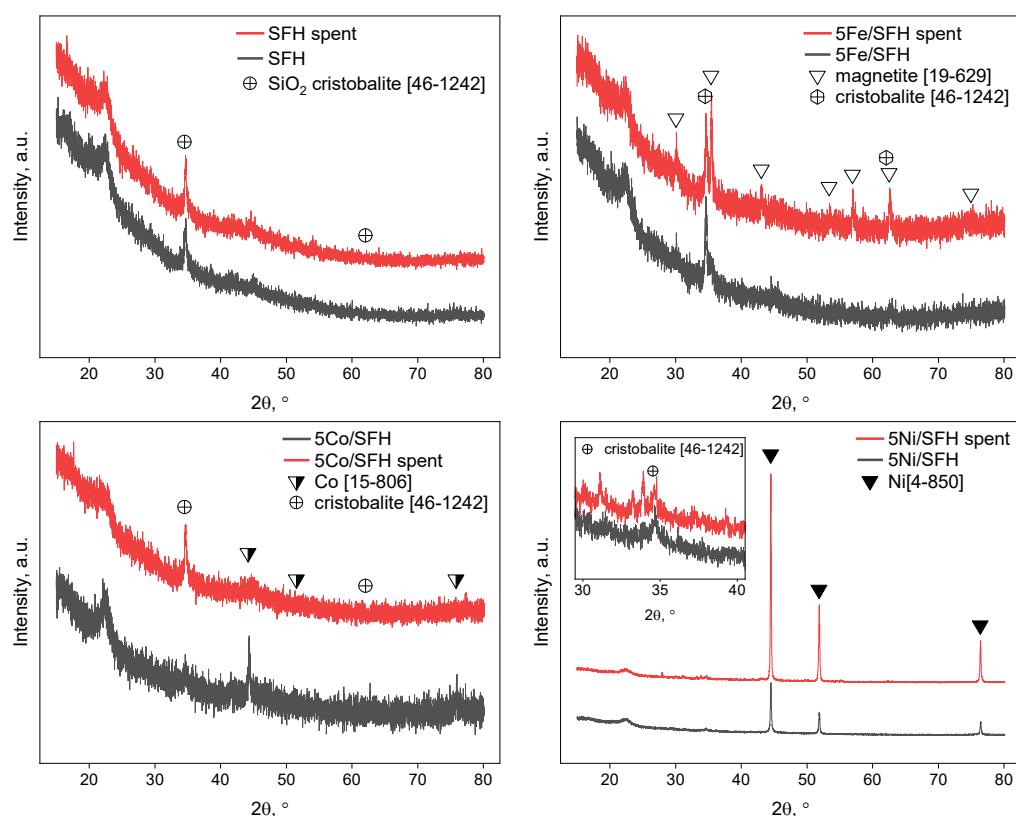
**Figure 8.** XRD patterns of the samples after 600 °C heating in a $CO_2$ flow and the patterns of these samples after the gasification catalytic tests. The inset picture is the enlarged patten of the Ni-loaded sample.

Fe-loaded samples demonstrate the pattern of the magnetite phase (the ICDD card number [19–629]) along with the cristobalite phase. The Co-loaded catalyst showed very weak reflexes of the phase of metallic Co (the ICDD card [15–806]) in both patterns for the sample after pre-heating at 600 °C in a $CO_2$ flow and after the catalytic test. Nevertheless, the crystallinities of these phases are not so good, and generally, all the mentioned samples are amorphous. The only well-crystallized samples are the Ni-loaded catalysts after preheating and after the catalytic test. The observed phase is metallic Ni ([4–850]). After pre-heating and after the catalytic test, the Ni crystallite sizes can be estimated using the Sherrer equation and the reflex of the (111) plane as 82 and 106 nm, respectively. Additionally, a very weak reflex of the cristobalite phase can be observed in the enlarged picture in Figure 8.

SAED patterns for fresh and spent samples are given in Figure 9. For the fresh iron-containing sample, the crystal phase of magnetite can be identified (the ICDD card number [19–629]). This is in accordance with the result of XRD examination. The spent sample contains probably Hagg carbide $Fe_{2.5}C$ according to the database (the ICDD card number [36–1248]), but we cannot see this phase via the XRD. SAED showed it most probably because of the locality of the method of examination. The pre-heated 'fresh' sample, according to the SAED spectrum, contains the phase of metallic cobalt (the ICDD card number [5–727]) already at the pre-heating conditions during the XRD examination (we still can see them but not so clearly). The spent sample does not show any crystal phases. The sample 5 Ni/SCF seems to contain the phase of nickel carbide $NiC_x$ (the ICDD card number [45–979]), but not all the reflexes are identified here. If so, it can be guessed that the reduction process involves the stage of carbide formation.
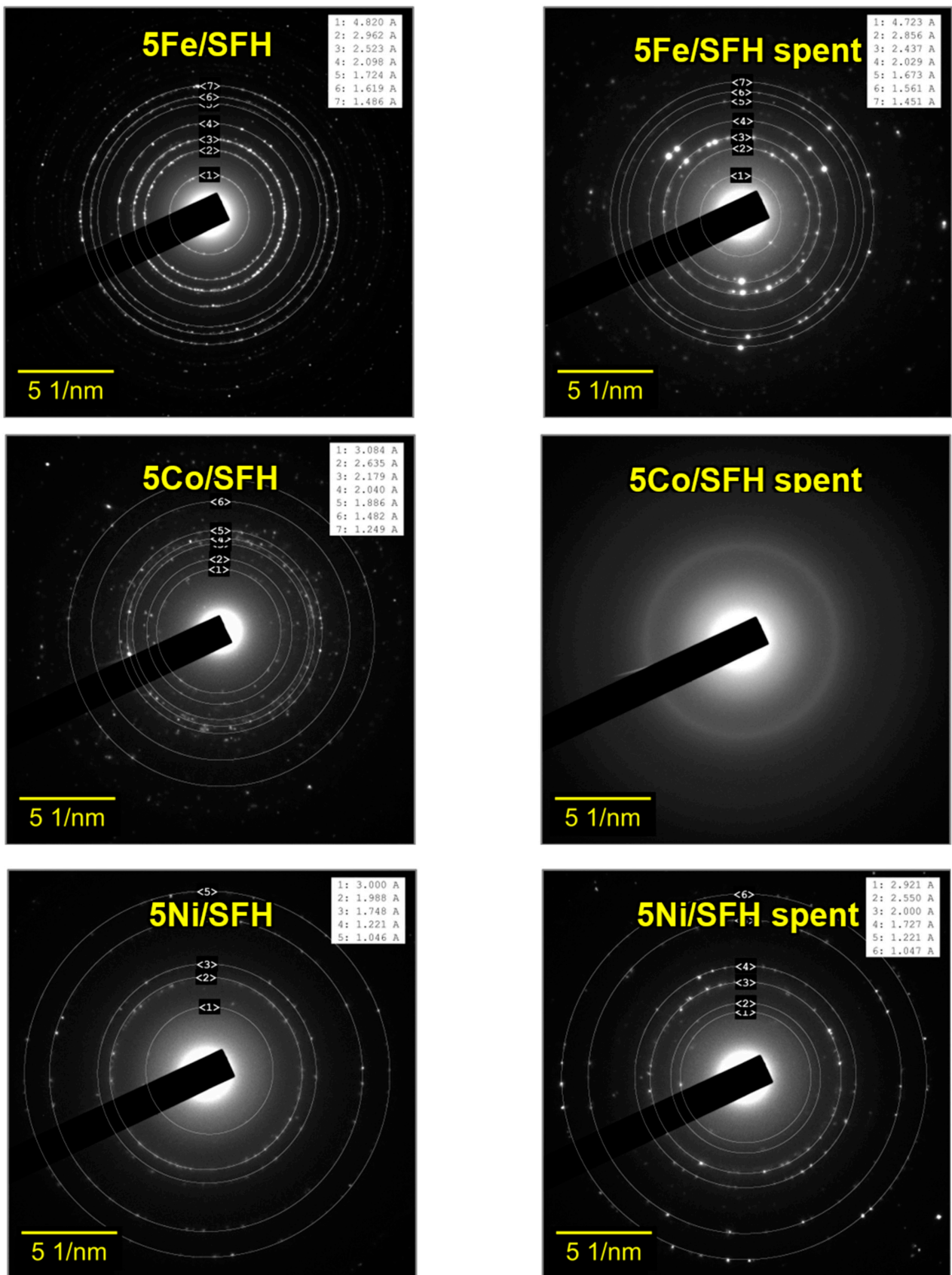
**Figure 9.** SAED patterns for the samples 5 Fe/SFH and 5 Ni/SFH, both fresh and spent. The sample 5 Co/SFH does not demonstrate any clear pattern (no rings shown here).

### 3.3. Catalytic Gasification

The results of the catalytic tests in the process of $CO_2$-assisted gasification are shown in Figure 10. It is interesting to note that the superior catalytic behavior of the Ni-loaded sample was found only at the metal loading of 1 wt. %, while the activity is still good at the loadings of 3 and 5 wt. %, but the Co-loaded samples showed much higher $CO_2$ conversions. The nature of such a phenomenon may be related to the difference in the metal nature and the structural features. The Ni-loaded sample demonstrated larger particles on the surface and appeared to be the among the active catalysts. While Co shows smaller particles, its activity is rather similar; therefore, it can be suggested that Co and Ni are the most active naturally. Additionally, the effect of Ni was also the highest conversion level during 1% loading of the metal. It appeared to be enough for the formation of an active phase.
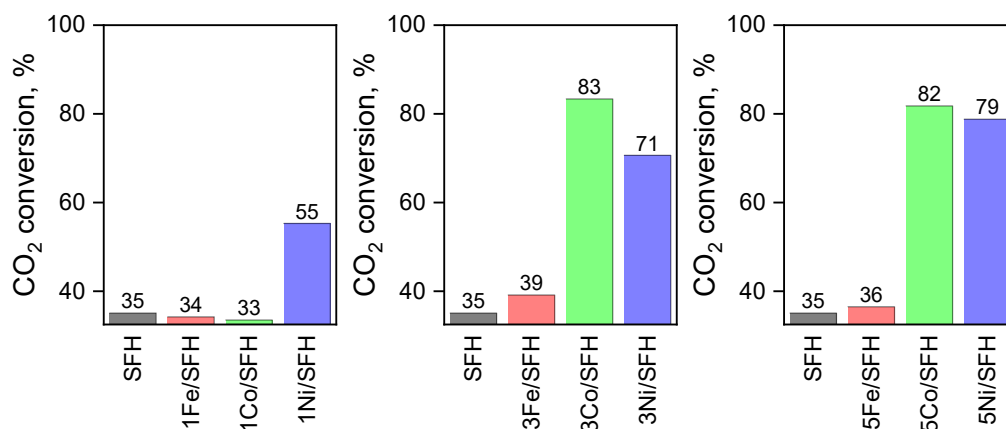


**Figure 10.** The results of the catalytic tests for the prepared metal-loaded materials and the starting sunflower husk in the reaction of $CO_2$-assisted gasification at 800 °C.

The loading of the samples with iron leads to no significant difference in the activity in carbon-dioxide-assisted gasification. The difference between the $CO_2$ conversions in the cases of 3 and 5 wt. % metal is not large, but in the case of the sample loaded with cobalt, it is negligible, while the Ni-containing sample increases the conversion of $CO_2$ for 8%. It can be tentatively explained by much smaller metal particles in the cobalt-containing sample, and thus a larger fraction of the metal is available on the surface of the material. So, it seems that the only parameter affecting the activity of the Co- and Ni-containing samples is the metal particle size, while iron is poorly active.

Only slight changes in the particle size distribution for the sample loaded with iron can be explained by its hardly noticeable participation in the catalytic process (the observed activity is approximately the same as it was without iron added). The difference in the Co- and Ni-loaded samples behavior does not imply such correlation with the catalytic results and likely can be explained by the difference in the metal nature.

To estimate the overall yields of CO, the curves of $CO_2$ conversion were integrated and normalized to 100% of the area in units of the product of temperature and time. It can be seen that the yields of CO attained for these samples are decreasing in the following order, while metal loading was 3 and 5 wt. %: Co > Ni > Fe, whereas for the loading of 1 wt. %, the order was slightly different: Ni > Co ≈ Fe > blank SFH (Figure 11). The data are similar to those for the conversion of $CO_2$.

Additionally, the material balance was closed, it was revealed that the observed products are the majority of carbon atoms entered into the reactor, and the fraction of them was higher than 85% for all the samples. The composition of liquid products is given in Table 3. An example of fitted curves is shown in Figure 12. The resulting areas were used to calculate the material balance, and it was shown that the resulting detected gas mixture compositions correspond to quite a good convergence. Since the most pronounced drop in

particle size was observed for the Co-containing sample, the highest effectiveness (yield) was obtained. That reason also supports the idea of the carbide mechanism of the process, which resulted in the formation of small particles of metallic cobalt.
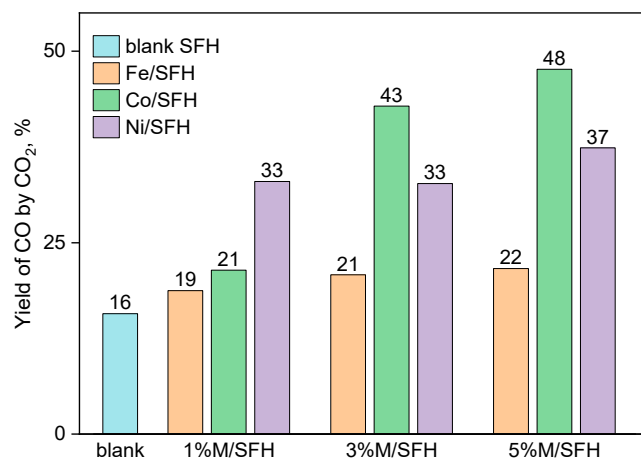


**Figure 11.** Yields of CO calculated on the basis of carbon dioxide converted for the prepared metal-loaded materials and the starting sunflower husk in the reaction of $CO_2$-assisted gasification at 500–800 °C.

**Table 3.** CHNOS analysis results for liquid products of gasification of sunflower husk.

| Sample | $w(C)$, wt. % | $w(H)$, wt. % | $w(N)$, wt. % |
|---|---|---|---|
| SFH | 29.6 | 5.4 | 5.3 |
| 1 Fe/SFH | 60.6 | 6.2 | 2.1 |
| 1 Co/SFH | 59.6 | 6.1 | 1.5 |
| 1 Ni/SFH | 58.8 | 6.1 | 1.7 |

Sulfur was not detected for all the samples.
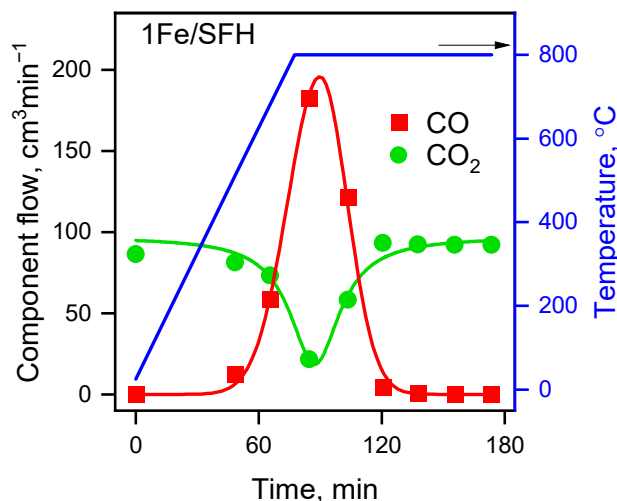


**Figure 12.** An example of the component flows fitting. Green and red legends reflect to carbon dioxide and carbon monoxide components flows respectively. The blue legend reflects temperature in Celsius degree.

## 4. Conclusions

The biomass (sunflower husk) was studied as a source of CO produced by $CO_2$-assisted gasification and as a way to utilize $CO_2$ and organic wastes produced from a harvest. Iron-, cobalt-, and nickel-based materials were investigated in the process of $CO_2$-assisted gasification of sunflower husk. The Co-based catalyst with 3 and 5 wt. % of Co demonstrates the best activity among the studied materials ($CO_2$ conversion was up to 83%). The possible reason for such superiority of the Co catalyst may be explained by the fact that Ni compounds lead to the formation of the metallic nickel phase and thus lose the active surface area and that is why they cannot further enhance the $CO_2$ conversion rate effectively, while cobalt does not show such a formation of well-crystallized metal particles. The observed layered structure of the particles evidenced the migration of Ni atoms through the particles of the carbon material. No significant differences in the composition of the surface of the samples before and after the catalytic tests were observed.

## Abbreviations

| | |
|---|---|
| ICDD | The International Center for Diffraction Data |
| SAED | selected area electron diffraction |
| XRD | X-ray diffraction |
| SEM | scanning electron microcopy |
| EDX | energy-dispersive spectroscopy |
| TEM | transmission electron microcopy |
| SFH | sunflower husk. |

## References

1. Nyambuu, U.; Semmler, W. Fossil Fuel Resource Depletion, Backstop Technology, and Renewable Energy. In *Sustainable Macroeconomics, Climate Risks and Energy Transitions: Dynamic Modeling, Empirics, and Policies*; Springer: Cham, Switzerland, 2023; pp. 71–85. [CrossRef]
2. Medvedev, A.A.; Kustov, A.L.; Beldova, D.A.; Kravtsov, A.V.; Kalmykov, K.B.; Sarkar, B.; Kostyukhin, E.M.; Kustov, L.M. Gasification of hydrolysis lignin with $CO_2$ in the presence of Fe and Co compounds. *Mendeleev Commun.* **2022**, *32*, 402–404. [CrossRef]
3. Medvedev, A.A.; Kustov, A.L.; Beldova, D.A.; Kalmykov, K.B.; Mashkin, M.Y.; Shesterkina, A.A.; Dunaev, S.F.; Kustov, L.M. Influence of the Method of Fe Deposition on the Surface of Hydrolytic Lignin on the Activity in the Process of Its Conversion in the Presence of $CO_2$. *Int. J. Mol. Sci.* **2023**, *24*, 1279. [CrossRef] [PubMed]
4. Medvedev, A.A.; Kustov, A.L.; Beldova, D.A.; Polikarpova, S.B.; Ponomarev, V.E.; Murashova, E.V.; Sokolovskiy, P.V.; Kustov, L.M. A Synergistic Effect of Potassium and Transition Metal Compounds on the Catalytic Behaviour of Hydrolysis Lignin in $CO_2$-Assisted Gasification. *Energies* **2023**, *16*, 4335. [CrossRef]

5. Beldova, D.A.; Medvedev, A.A.; Kustov, A.L.; Mashkin, M.Y.; Kirsanov, V.Y.; Vysotskaya, I.V.; Sokolovskiy, P.V.; Kustov, L.M. $CO_2$-Assisted Sugar Cane Gasification Using Transition Metal Catalysis: An Impact of Metal Loading on the Catalytic Behavior. *Materials* **2023**, *16*, 5662. [CrossRef]

6. Lopez, G.; Santamaria, L.; Lemonidou, A.; Zhang, S.; Wu, C.; Sipra, A.T.; Gao, N. Hydrogen generation from biomass by pyrolysis. *Nat. Rev. Methods Prim.* **2022**, *2*, 20. [CrossRef]

7. Czerski, G.; Śpiewak, K.; Grzywacz, P.; Wierońska-Wiśniewska, F. Assessment of the catalytic effect of various biomass ashes on $CO_2$ gasification of tire char. *J. Energy Inst.* **2021**, *99*, 170–177. [CrossRef]

8. Ye, D.; Agnew, J.; Zhang, D. Gasification of a South Australian low-rank coal with carbon dioxide and steam: Kinetics and reactivity studies. *Fuel* **1998**, *77*, 1209–1219. [CrossRef]

9. Matsunami, J.; Yoshida, S.; Oku, Y.; Yokota, O.; Tamaura, Y.; Kitamura, M. Coal gasification by $CO_2$ gas bubbling in molten salt for solar/fossil energy hybridization. *Sol. Energy* **2000**, *68*, 257–261. [CrossRef]

10. Popa, T.; Fan, M.; Argyle, M.D.; Slimane, R.B.; Bell, D.A.; Towler, B.F. Catalytic gasification of a Powder River Basin coal. *Fuel* **2013**, *103*, 161–170. [CrossRef]

11. Namkung, H.; Yuan, X.; Lee, G.; Kim, D.; Kang, T.-J.; Kim, H.-T. Reaction characteristics through catalytic steam gasification with ultra clean coal char and coal. *J. Energy Inst.* **2014**, *87*, 253–262. [CrossRef]

12. Alam, M.; DebRoy, T. Reaction between $CO_2$ and coke doped with NaCN. *Carbon* **1987**, *25*, 279–288. [CrossRef]

13. Devi, T.G.; Kannan, M. Calcium catalysis in air gasification of cellulosic chars. *Fuel* **1998**, *77*, 1825–1830. [CrossRef]

14. Chen, S.; Yang, R. Mechanism of alkali and alkaline earth catalyzed gasification of graphite by $CO_2$ and $H_2O$ studied by electron microscopy. *J. Catal.* **1992**, *138*, 12–23. [CrossRef]

15. Hengel, T.D.; Walker, P.L. Catalysis of lignite char gasification by exchangeable calcium and magnesium. *Fuel* **1984**, *63*, 1214–1220. [CrossRef]

16. Kurbatova, N.A.; El'man, A.R.; Bukharkina, T.V. Application of catalysts to coal gasification with carbon dioxide. *Kinet. Catal.* **2011**, *52*, 739–748. [CrossRef]

17. Kodama, T.; Funatoh, A.; Shimizu, K.; Kitayama, Y. Kinetics of metal oxide-catalyzed $CO_2$ gasification of coal in a fluidized-bed reactor for solar thermochemical process. *Energy Fuels* **2001**, *15*, 1200–1206. [CrossRef]

18. Furimsky, E.; Sears, P.; Suzuki, T. Iron-Catalyzed Gasification of Char in $CO_2$. *Energy Fuels* **1988**, *2*, 634–639. [CrossRef]

19. Figueiredo, J.; Rivera-Utrilla, J.; Ferro-Garcia, M. Gasification of active carbons of different texture impregnated with nickel, cobalt and iron. *Carbon* **1987**, *25*, 703–708. [CrossRef]

20. Gokon, N.; Hasegawa, N.; Kaneko, H.; Aoki, H.; Tamaura, Y.; Kitamura, M. Photocatalytic effect of ZnO on carbon gasification with $CO_2$ for high temperature solar thermochemistry. *Sol. Energy Mater. Sol. Cells* **2003**, *80*, 335–341. [CrossRef]

21. Kuchinskaya, T.; Mamian, L.; Knyazeva, M.; Maximov, A. Hydrodeoxygenation of lignin-derived diphenyl ether on in situ prepared NiMoS catalyst: The effect of sulfur addition on catalyst formation. *Appl. Catal. A Gen.* **2023**, *663*, 119303. [CrossRef]

22. Koklin, A.E.; Bobrova, N.A.; Bogdan, T.V.; Mishanin, I.I.; Bogdan, V.I. Conversion of Phenol and Lignin as Components of Renewable Raw Materials on Pt and Ru-Supported Catalysts. *Molecules* **2022**, *27*, 1494. [CrossRef] [PubMed]

23. Bazhenova, M.A.; Kulikov, L.A.; Makeeva, D.A.; Maximov, A.L.; Karakhanov, E.A. Hydrodeoxygenation of Lignin-Based Compounds over Ruthenium Catalysts Based on Sulfonated Porous Aromatic Frameworks. *Polymers* **2023**, *15*, 4618. [CrossRef] [PubMed]

24. Yu, H.; Wu, Z.; Chen, G. Catalytic gasification characteristics of cellulose, hemicellulose and lignin. *Renew. Energy* **2018**, *121*, 559–567. [CrossRef]

25. Pan, Y.; Tursun, Y.; Abduhani, H.; Turap, Y.; Abulizi, A.; Talifua, D. Chemical looping gasification of cotton stalk with bimetallic Cu/Ni/olivine as oxygen carrier. *Int. J. Energy Res.* **2020**, *44*, 7268–7282. [CrossRef]

26. Ruiz, M.; Schnitzer, A.; Courson, C.; Mauviel, G. Fe-doped olivine and char for in-bed elimination of gasification tars in an air-blown fluidised bed reactor coupled with oxidative hot gas filtration. *Carbon Resour. Convers.* **2022**, *5*, 271–288. [CrossRef]

27. Mastuli, M.; Kamarulzaman, N.; Kasim, M.; Sivasangar, S.; Saiman, M.; Taufiq-Yap, Y. Catalytic gasification of oil palm frond biomass in supercritical water using MgO supported Ni, Cu and Zn oxides as catalysts for hydrogen production. *Int. J. Hydrogen Energy* **2017**, *42*, 11215–11228. [CrossRef]

28. Irfan, M.; Li, A.; Zhang, L.; Ji, G.; Gao, Y.; Khushk, S. Hydrogen-rich syngas from wet municipal solid waste gasification using Ni/Waste marble powder catalyst promoted by transition metals. *Waste Manag.* **2021**, *132*, 96–104. [CrossRef]

29. Irfan, M.; Li, A.; Zhang, L.; Wang, M.; Chen, C.; Khushk, S. Production of hydrogen enriched syngas from municipal solid waste gasification with waste marble powder as a catalyst. *Int. J. Hydrogen Energy* **2019**, *44*, 8051–8061. [CrossRef]

30. Bhattacharjee, N.; Biswas, A.B. Catalytic pyrolysis of rice husk with $SnCl_2$, $Al_2O_3.4SiO_2.H_2O$, and $MoS_2$ for improving the chemical composition of pyrolysis oil and gas. *J. Indian Chem. Soc.* **2022**, *99*, 100728. [CrossRef]

31. Anisimova, O.S.; Kolomytsa, V.A. Biofuel productuin from sunflower husk. *IOP Conf. Ser. Earth Environ. Sci.* **2021**, *659*, 012115. [CrossRef]

32. Cui, X.; Yang, J.; Shi, X.; Lei, W.; Huang, T.; Bai, C. Pelletization of Sunflower Seed Husks: Evaluating and Optimizing Energy Consumption and Physical Properties by Response Surface Methodology (RSM). *Processes* **2019**, *7*, 591. [CrossRef]

33. Kanatli, T.K.; Ayas, N. Gasification of sunflower seed pulp for the synthesis of hydrogen-rich products. *Int. J. Smart Grid Clean Energy* **2019**, *8*, 226–230. [CrossRef]

34. Chun, D.D.; Ni, D.; Simson, A. The effect of inherent inorganics and $CO_2$ co-pyrolysis on biochar production from biowastes and their gasification reactivity. *Biomass Bioenergy* **2022**, *158*, 106361. [CrossRef]
35. Lobo, L.S.; Carabineiro, S.A. Kinetics and mechanism of catalytic carbon gasification. *Fuel* **2016**, *183*, 457–469. [CrossRef]